IMPACT OF TIDAL STREAM ENERGY EXPLOITATION ON ESTUARINE HYDRODYNAMICS

M. Sanchez[1], R.Carballo[1], V.Ramos[1], A. Vazquez[1], M. Alvarez[1], G.Iglesias[2]

During the last years there has been an increasing interest towards the exploitation of marine energies and, in particular, of tidal stream energy. Although the impact of tidal stream farms is expected to be much lesser than that the conventional barrages, there are numerous environmental variables likely to be altered. This is of particular interest in the case of the Galician Rias that present complex 3D flow patterns, which is one of the main causes of their large oceanic productivity. Therefore, its modification as a result of tidal energy exploitation should be analysed by means of 3D modelling. The present study investigates the environmental impacts of tidal energy extraction in the Ria de Ortigueira located in the NW of Spain. For this purpose, a numerical model was implemented in Ria de Ortigueira (NW Spain), a promising region for tidal stream energy exploitation. First, the model was successfully validated on the basis of field measurements of water levels and magnitude and direction of the tidal currents, then, it was used to describe the potential effects resulting from the operation of a previously proposed tidal stream farm during typical winter and summer conditions. For this purpose, the momentum sink approach was used. Overall, it was found that the resulting transient flow modifications were concentrated in the vicinity of the farm, with nearly negligible effects outside the inner ria. Furthermore, important asymmetry effects were also observed; although the inner part of the estuary is flood dominated, the complex geometry of this area causes that the most important effects occur during the ebb with modifications of up to 15 % of the unaltered flow, which represent an impact almost twice as strong as that during the flood. Finally, the effects on the residual flow are of the same order, in terms of percentage of velocity variation, as in the case of the transient flow; however, they extend over a wider region, affecting the middle ria, where a complex 3D circulation pattern (a positive estuarine circulation) develops.

Keywords: Tidal stream energy impact; 3D numerical modelling; transient circulation; residual circulation

[1] Univ. of Santiago de Compostela, Hydraulic Eng., Campus Univ. s/n, 27002 Lugo, Spain
[2] University of Plymouth, School of Marine Science and Engineering, Marine Building, Drakes Circus, Plymouth PL4 8AA, United Kingdom

1. Introduction

In recent years, the rising world-wide energy demand has brought an increase in the use of carbon-free and renewable energy sources. In this context, several policies are enshrined. Among them, EU's directive 2009/28/EC (European Commission 2012), which aims to supply the 20 % of the electric demand from renewable sources by 2020, stands out. Within the wide variety of renewable energy sources, marine energies have been increasingly gaining interest during the last years (Bahaj 2011, 3399-3416). Among them, tidal stream energy, which taps the kinetic energy contained in the tidal currents, is arising as an alternative energy source (Ramos et al. 2014, 432-444; Blunden and Bahaj 2006, 121-132; Carballo, Iglesias, and Castro 2009, 1517-1524). Tidal streams are generated in coastal regions by the tide-driven variation of the sea level and can be locally amplified by the coastline shape and bathymetry. Among the main advantages of tidal stream energy in comparison with other renewable sources are: (i) the high predictability of the resource, (ii) absence of extreme flows (unlike wind energy), (iii) high load factors and (iv) low visual and land occupation. On the other hand, the main disadvantages are: (i) the technology of tidal energy converters is at the early stage of development, which is reflected in the fact that with only a few tidal farms are in operation at present and (ii) the possible disruptions that may be caused on the marine environment(Neill, Jordan, and Couch 2012, 387-397; Ahmadian and Falconer 2012, 318-327; Ahmadian, Falconer, and Lin 2010, 107-117; Sanchez et al. 2014, 691-701).

In addition, the understanding of the potential impacts on the marine environment of the extraction of energy from the tidal flow is far from complete (Sanchez et al. 2014, 691-701). Recent research has shown that the operation of a tidal farm may alter both the transient and residual circulations. These alterations may be noticeable at considerable distances from the farm, from tens to hundreds of kilometers for the transient and residual circulation, respectively; consequently, numerous variables related to the circulation patterns such as sediment transport rates, pollutant dispersion and nutrient concentrations may be affected. Moreover, the 3D circulation patterns, which are present in many estuaries may also be altered by the operation of a tidal farm. The present study assesses the 3D impacts of a tidal stream farm on the transient and residual circulation of an estuary in a case study: Ria de Ortigueira (Figure 1), Galicia (NW Spain). In addition, it is important to point out that the residual circulation plays a major role in the Galician rias; it explains their high biological productivity, which forms the basis of an important aquaculture and fishing industry(Carballo, Iglesias, and Castro 2009, 130; Iglesias and Carballo 2009, 94-108).

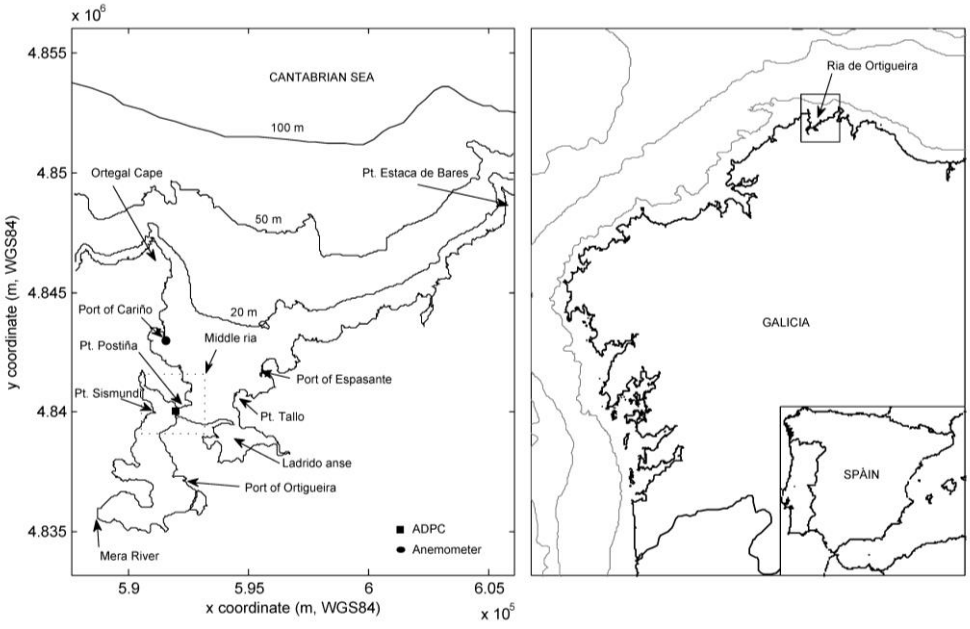

Figure 1. Location of Ria de Ortigueira in the North of Spain

Ria de Ortigueira, one of the largest Rias Altas, is composed of four lobes. The largest by far is the outermost (or third) lobe, a broad embayment between two major headlands, Cape Ortegal and Pt. Estaca de Bares (Figure 1). The middle (or second) lobe, much smaller, is limited by Pt. Descada (also known as Pt. Sartán) and Pt. Tallo. Finally, the inner (or first) lobe is extremely complex, with two well- differentiated parts to the east and west, the Ladrido anse and the Ria de Santa Marta de Ortigueira, respectively. The main discharge into the ria is River Mera, with an average flow rate of 5.45 m^3 there are also a number of streams flowing into the ria, but with very minor discharges. The morphology of the ria, its sizeable surface area (85 km^2) and substantial tidal range (with a maximum value of 4.5 m) combine to produce a significant tidal potential.

This investigation was carried out by means of a 3D numerical model of the ria hydrodynamics, successfully validated based on field data (Section 2). After validation, the model was used to simulate the operation of a tidal farm at a site of interest. The site was chosen by means of the TSE index, a tool that was recently put forward (Iglesias et al. 2012, 350-357) to simplify the selection of tidal stream sites in depth-limited areas. The extraction of energy from the flow by the tidal farm was accounted for in the model by adding a sink term to the local momentum equations. The model was then applied to examine the impacts of the farm on the transient and residual circulation patterns in the estuary in two cases, representative of typical winter and summer conditions (Section 3). Conclusions are drawn in Section 4.

2. Materials and methods

2.1. Numerical model

The numerical model used for the present study, Delft3D-FLOW, is a finite difference code which solves the 3D baroclinic Navier-Stokes and transport equations under the shallow-water and Boussinesq assumptions. Therefore, the equations solved by the model are:

(i) The continuity equation:

$$\frac{\partial u}{\partial x}+\frac{\partial v}{\partial y}+\frac{\partial w}{\partial z}=Q \qquad (1)$$

where, x, y and z represent the east, north and vertical axes, respectively; u, v and w are the velocity components on those directions and Q represents the intensity of mass sources per unit area.

(ii) Momentum equations in horizontal direction:

$$\left\{\begin{array}{l}\dfrac{Du}{Dt}=fv-g\dfrac{\partial \zeta}{\partial x}-\dfrac{g}{\rho_0}\displaystyle\int_{z'=z}^{z'=\zeta}\frac{\partial \rho}{\partial x}dz'+\upsilon_h\left(\frac{\partial^2 u}{\partial x^2}+\frac{\partial^2 u}{\partial y^2}\right)+\upsilon_v\left(\frac{\partial^2 u}{\partial z^2}\right)\\ \dfrac{Dv}{Dt}=-fu-g\dfrac{\partial \zeta}{\partial y}-\dfrac{g}{\rho_0}\displaystyle\int_{z'=z}^{z'=\zeta}\frac{\partial \rho}{\partial y}dz'+\upsilon_h\left(\frac{\partial^2 v}{\partial x^2}+\frac{\partial^2 v}{\partial y^2}\right)+\upsilon_v\left(\frac{\partial^2 v}{\partial z^2}\right)\end{array}\right\} \qquad (2)$$

where, ζ is the free surface elevation relative to a reference plane ($z = 0$), f is the Coriolis parameter; g is the gravitational acceleration, υ_h and υ_v are the horizontal and vertical eddy viscosity coefficients, respectively; and ρ and ρ_o are the density and the reference density of sea water, respectively.

(iii) Momentum equation in vertical direction:

Under the shallow water assumption, the vertical momentum equation is reduced to a hydrostatic pressure (p) equation:

$$\frac{\partial p}{\partial z} = -\rho g \qquad (3)$$

(iv) Transport equation

$$\frac{Dc}{Dt} = D_h\left(\frac{\partial^2 c}{\partial x^2} + \frac{\partial^2 c}{\partial y^2}\right) + D_v \frac{\partial^2 c}{\partial z^2} - \lambda_d c + R_s \qquad (4)$$

where, c stands for salinity or temperature; D_h and D_v are the horizontal and vertical eddy diffusivity coefficients, respectively; λ_d represents the first order decay process; and R_s is the source term per unit area. This equation is solved both for salinity and temperature.

2.2. Model implementation in Ria de Ortigueira

The bathymetry of the ria (Figure 2) was digitised from nautical charts 408 and 4083 of the Navy Hydrographic Office (Instituto Hidrográfico de la Marina). The horizontal grid resolution was set to 50 × 50 m within the constricted channels, of interest for tidal energy exploitation, and increased gradually beyond the 25 m contour in the middle ria, towards the north grid boundary (Figure 2). The shallow areas of the upper ria represent a modelling challenge due to the presence of tidal flats and their alternate drying and flooding. In the present work these areas are fully included within the computational grid. For this purpose, data from a digital terrain model with a resolution of 10 × 10 m was also included.

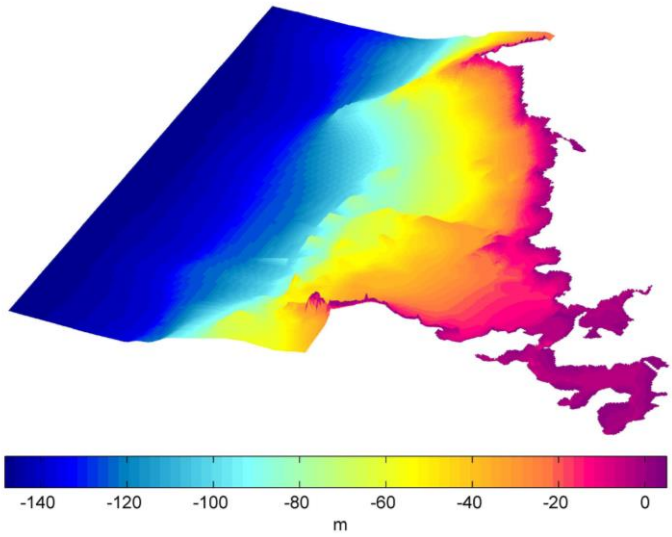

Figure 2. Bathymetry of Ria de Ortigueira

For the horizontal discretization the Arakawa C-grid was used, a staggered grid in which water levels ζ and velocities (u and v) are computed at the centrepoints of grid cells and velocities are computed at the mid points of grid cell faces, respectively. The discretization of the horizontal advection terms in the momentum and transport equations was computed by means of the Cyclic method. For the vertical discretization, a boundary fitted σ-coordinate was used. Twelve σ-layers were prescribed, with the following thickness (% of the local water depth) from bottom to surface: 2,3,5,10,15,15,15,15,15,10,5,3,2 (Carballo, Iglesias, and Castro 2009, 130). In this manner the grid resolution was higher near the surface and the bed aiming a better modeling of the boundary layer flows.

Along the ocean boundary a Diriclet boundary condition was imposed with the sea water level as a function of time. The sea level was computed using the major tidal harmonics, which were obtained from the global ocean tide model TPXO 7.2 (Egbert, Bennett, and Foreman 1994, 24821-52)(Table1).

Table1. Seven major tidal armonics		
	Amplitude (cm)	Phase (º)
M2	122.8	90.1
S2	42.9	121.1
N2	26.0	70.4
K2	12.0	118.7
K1	7.3	73.5
O1	6.2	324.6
P1	2.2	65.2
Q1	2.1	271.3

The boundary conditions at the land margins were null velocity and free slip (zero shear stress). Salinity and temperature were prescribed at the ocean boundary (Table 2) according to the data obtained from the Spanish Institute of Oceanography.

Table2. Sal. Temp ocean boundary	
Salinity (ppt)	Temperature (ºC)
35.348	15.789

2.3. Numerical modeling of the tidal energy extraction: the momentum sink approach

The operation of a TEC was simulated by introducing new terms (momentum sink terms, M_x and M_y), into the x and y momentum equations (Ahmadian, Falconer, and Bockelmann-Evans 2012, 107-116):

$$\left\{\begin{array}{l} \dfrac{Du}{Dt} = fv - g\dfrac{\partial\zeta}{\partial x} - \dfrac{g}{\rho_0}\displaystyle\int_{z'=z}^{z'=\zeta}\frac{\partial\rho}{\partial x}dz' + \upsilon_h\left(\frac{\partial^2 u}{\partial x^2}+\frac{\partial^2 u}{\partial y^2}\right)+\upsilon_v\left(\frac{\partial^2 u}{\partial z^2}\right)+M_x \\ \dfrac{Dv}{Dt} = -fu - g\dfrac{\partial\zeta}{\partial y} - \dfrac{g}{\rho_0}\displaystyle\int_{z'=z}^{z'=\zeta}\frac{\partial\rho}{\partial y}dz' + \upsilon_h\left(\frac{\partial^2 v}{\partial x^2}+\frac{\partial^2 v}{\partial y^2}\right)+\upsilon_v\left(\frac{\partial^2 v}{\partial z^2}\right)+M_y \end{array}\right\} \quad (5)$$

These two new momentum terms can be expressed as:

$$\left\{\begin{array}{l} M_x = \dfrac{F_x}{\rho} \\ M_y = \dfrac{F_y}{\rho} \end{array}\right\} \quad (6)$$

Where, F_x and F_y are, respectively, the component in the x and y directions of the flow retarding force per unit volume V due to the presence of an energy device. These components have the same magnitude as, and opposite direction to, the thrust force, F_T, i.e. the force exerted by the flow on the device; therefore the momentum contribution can be expressed as:

$$\left\{\begin{array}{l} M_x = -\dfrac{1}{2}\dfrac{C_T A}{V}Uu \\ M_y = -\dfrac{1}{2}\dfrac{C_T A}{V}Uv \end{array}\right\} \quad (7)$$

Where, A is the cross-sectional area of the turbine rotor, U is the magnitude of the flow velocity, V is the volume of control and C_T is the thrust coefficient.

3. Results

3.1. Model validation

For the purpose of model validation, numerical results of water level and flow velocity and direction were compared with measured data obtained by means of an Acoustic Doppler Current Profiler (ADCP) from 16.XII.10 to 3.I.11. The numerical simulation covered an additional month to include the spin-up period and thus ensure that the initial conditions do not affect the results during the period of interest. During this period, the forcing factors taken into account were, in addition to the tide (Table 1), daily river discharges, wind velocity and direction every 30 min recorded by an anemometer (Figure 1) and salinity and temperature at the open ocean boundary.

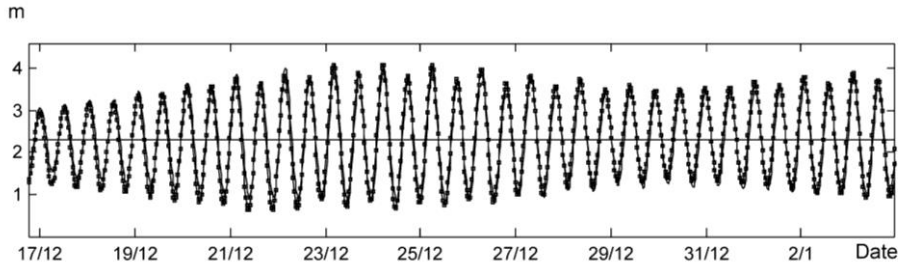

Figure 3. Comparison between computed and measured water levels in the ADCP location during validation period.

The agreement between observed and simulated water levels (Figure 3) was excellent, with a correlation coefficient (R) very close to unity (R=0.9895 (Table 2)). In the case of the flow velocity, prior to comparing computed and observed data, ADCP data were de-noised using a Stationary Wavelet Transform (SWT). Figure 4 shows the comparison for the surface, middle and bottom layers of the Eastward and Northward current velocities. On the whole it can be observed that there is a very good agreement in all layers; this is also indicated by the correlation coefficients computed, higher than 0.9, which indicates the capability of the model to properly simulate the flows in this ria.

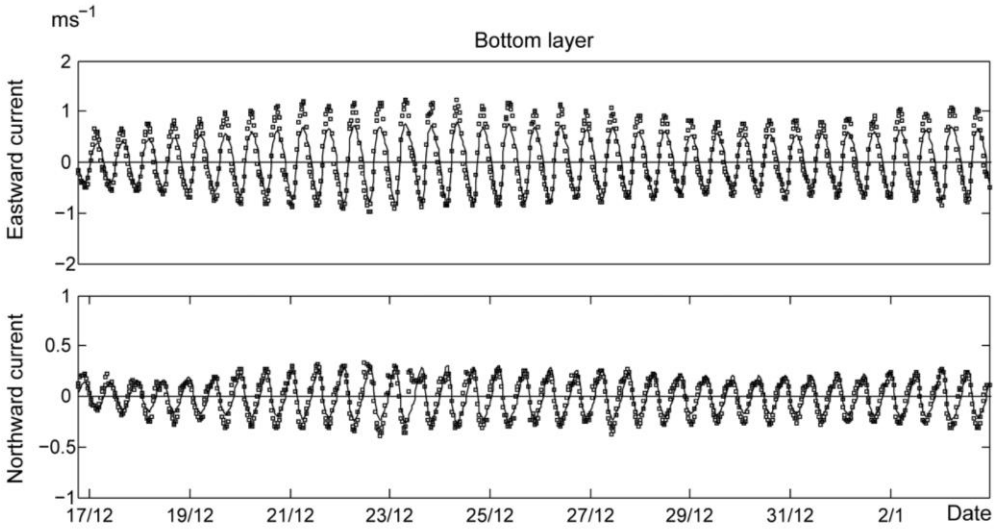

Figure 4a. Comparison between computed and measured current velocity in the ADCP location during validation period. (Bottom layer)

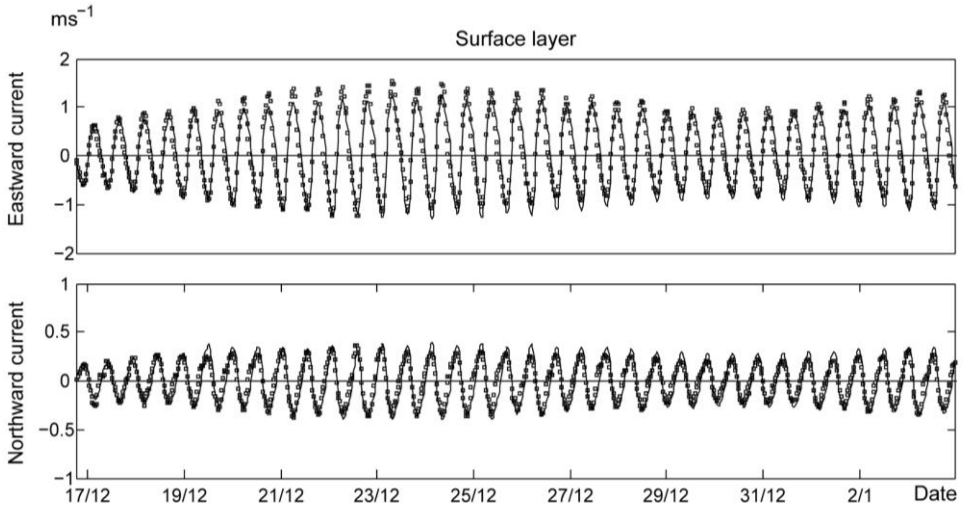

Figure 4. Comparison between computed and measured current velocity in the ADCP location during validation period.

3.2. Modelling of the tidal energy extraction in Ria de Ortigueira

Prior to investigate the environmental effects derived from the tidal stream energy extraction, the location for a prospective tidal stream plant was carried out by means of a new tool, the TSE index (Iglesias et al. 2012, 350-357), developed for this purpose in the case of areas with restricted water depths, such as the Galician Rias. The implementation of this tool in Ria de Ortigueira showed that the area with the highest potential for tidal energy exploitation is located in the inner ria, near the section in front of Pt. Postiña (Figure 1), with maximum flow velocities of around 2 ms^{-1} and 6 kW m^{-2} of power density. On these grounds, the site marked in Figure 5, with a total cross section of approx. 800 m^2. (100 m wide and 8 m deep), was selected (Iglesias et al. 2012, 350-357).

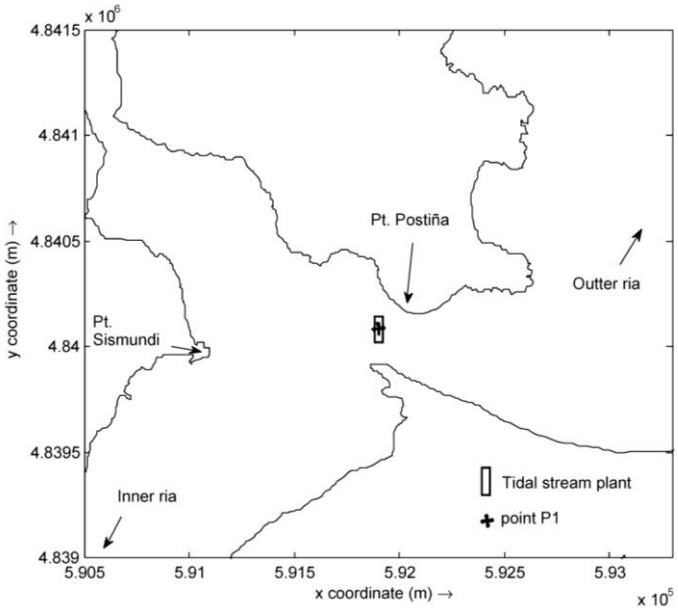

Figure 5. Location of the proposed tidal farm in Ria de Ortigueira

Having been defined the location and configuration of the tidal farm, the model was run for two characteristic cases of winter and summer conditions, without considering energy extraction in order to establish the baseline or reference conditions. Two additional cases, which take into account the energy extraction were also simulated. The model forcing in these cases comprised different conditions of river runoff, thermohaline conditions at the open boundaries and a common tidal forcing (Table 1). Winter conditions corresponded to the average of December, January and February, and summer conditions to the average of June, July and August. In the case of the river discharges, 8 m^3s^{-1} (winter average) and 3 m^3s^{-1} (summer average) were input to the model at the upper part of the inner ria; with respect to the themohaline conditions, they were prescribed based on the vertical profiles of temperature and salinity. Finally, as regards energy extraction, C_T was set to 1 following previous studies (Ahmadian and Falconer 2012, 318-327) which corresponds to C_p=0.4 (Myers and Bahaj 2010, 218-227) .

3.3. Impacts on the water levels

The water level variations due to the operation of the tidal farm are represented in Figure 6 for typical winter conditions. The differences between the winter and summer scenarios are negligible. It can be observed that the maximum water level differences occur, as could be expected, upstream in the vicinity of the tidal farm (East or West side during flood and ebb, respectively); these differences decrease as the distance to the farm increases – at a 5 km distance, the effects are hardly noticeable. The effects differ significantly depending on the moment of the tide; water level variations top 8 cm in the case of mid-ebb tide, and 2 cm in the case of mid-flood, in the order of previous tidal energy impact assessments. More generally, an important asymmetry emerges, in which the water level variations are of much greater importance during the ebb than during the flood, although in both situations the most affected area correspond to upstream where the water is retained by the farm – it represents an obstacle to the flow – and consequently water levels increase. Downstream, the variations, of lower importance, can be either positive or negative (predominantly negative).

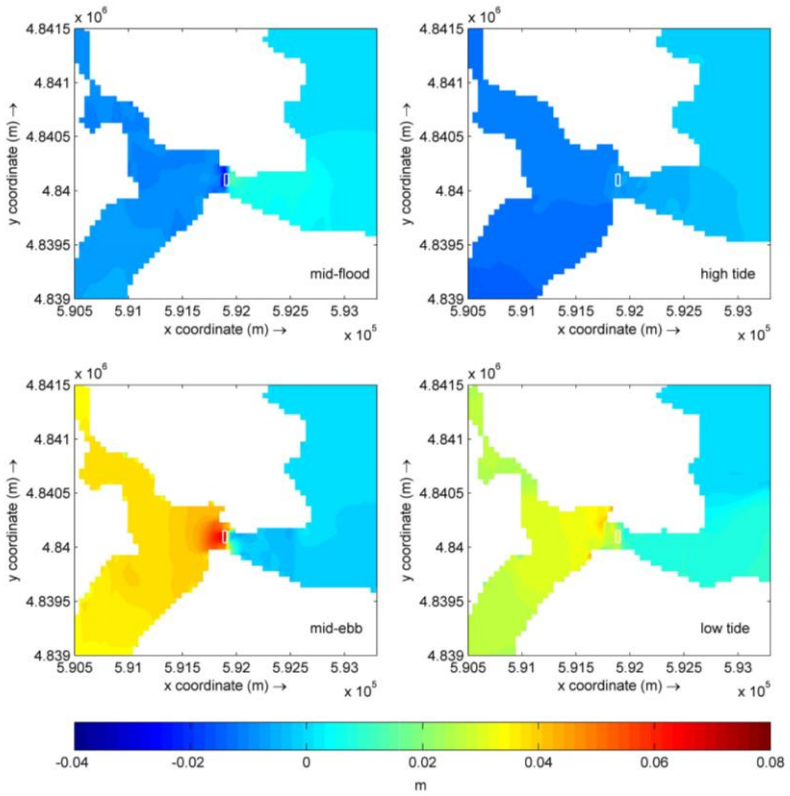

Figure 6. Water level differences between altered and unaltered conditions

3.4. Impacts on the transient circulation

The differences in the transient velocities with respect to the baseline situation were calculated at mid-ebb and mid-flood of a mean spring tide for winter and summer conditions. The differences between the winter and summer conditions are virtually non-existent, and, therefore in this section the typical winter conditions are used as a reference to assess the potential effects on the transient circulation. Figure 7 shows the difference of the velocity magnitude between the energy extraction case and the reference case in the surface and bottom layers (colour map), and the altered flow (vectors). The effects of the operation of the tidal farm on the transient circulation extend to more than 1 km distance; however, the major effects are basically restricted to the vicinity of the tidal farm (variations in the order of 0.1 - 0.2 ms^{-1}). The general pattern of the altered flow is similar throughout the water column but with somewhat lower magnitude in the bottom layer due to bed friction.

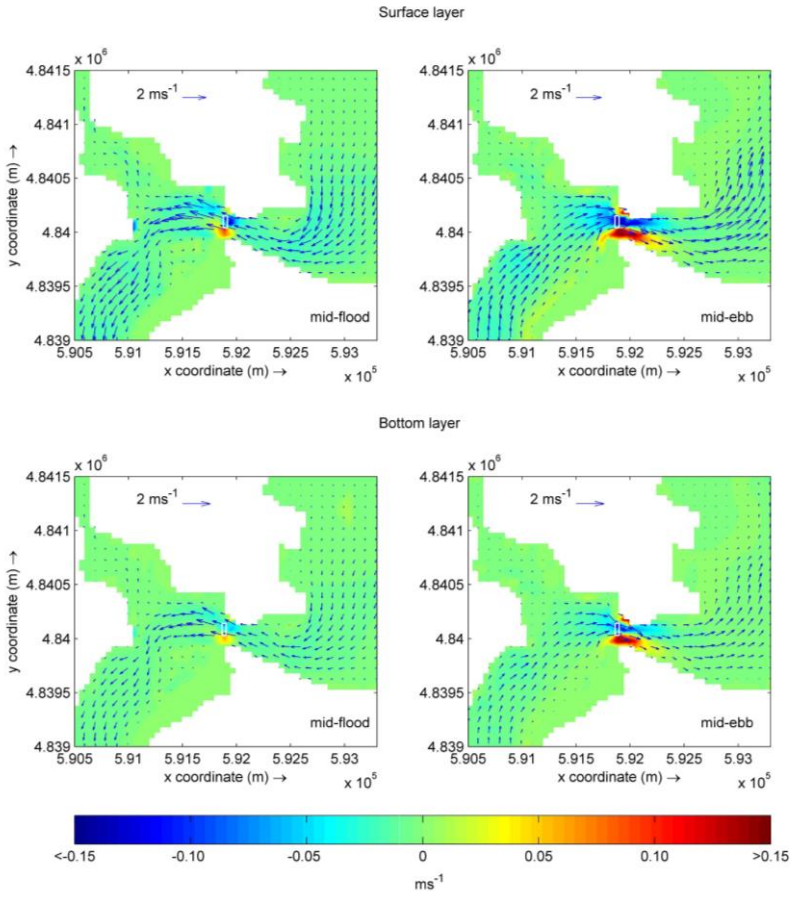

Figure 7. Transient velocity differences between altered and unaltered conditions

The reduction of the flow velocity is restricted to the area occupied by the farm and its projection following the direction of the main axis of the inner ria (East –West). The tidal farm tends to divert the flow, which is now redirected towards roughly the North and especially South sides of the farm, where the magnitude of the velocity increases. Naturally, there is a reduction of the available energy in the ria; nevertheless, the area where the velocity increases is in terms of total surface of similar importance to the area where the flow velocity decreases.

3.5. Impacts on the residual circulation

As mentioned in previous sections the residual patterns play a major in role in the Galician rias, and, therefore determining the impacts related to tidal stream energy exploitation presents a vital importance in order to ensure the future development of the tidal stream energy the Galician rias. In order to investigate this point, the estuarine residual circulation was computed for typical winter conditions during a full spring neap tidal cycle with and without considering energy extraction. Figure 8 shows the unaltered residual flow and Figure 9 shows the variation of the residual velocity magnitude between the energy extraction and the reference case (colour map), together with magnitude and direction of the altered residual flow (vectors).

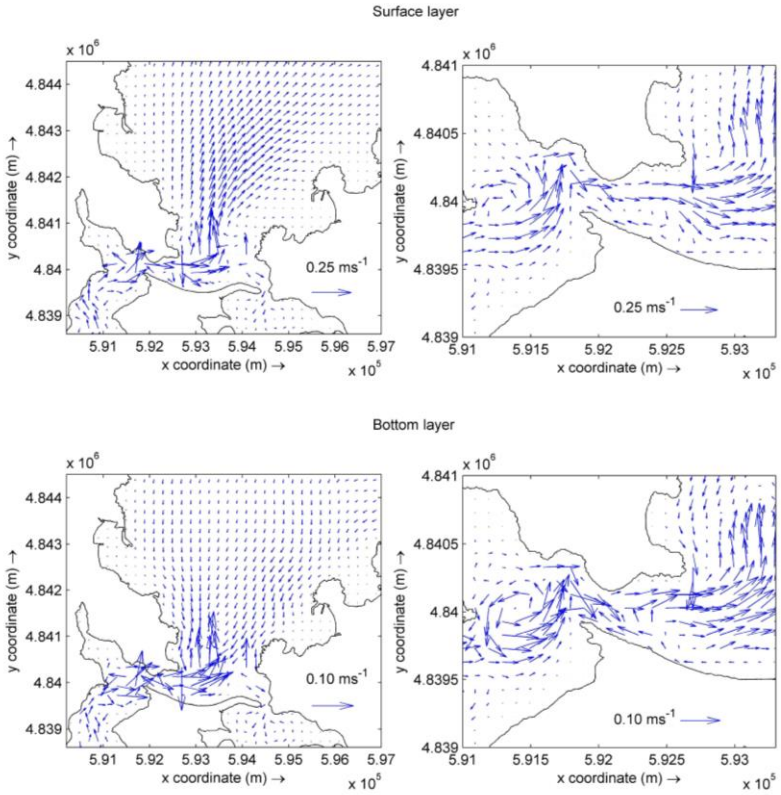

Figure 8. Unaltered residual circulation in Ria de Ortigueira

Two regions with different unaltered residual circulation pattern may be clearly distinguished. First, in the inner part of the ria, the residual velocity magnitude is higher and the general circulation pattern is similar throughout the water column. A residual eddy rotating counterclockwise is apparent in this area. Second, in roughly the middle and outer ria, the residual flow pattern corresponds, in general terms, to a positive estuarine circulation, with inflow of shelf water in the lower layers and outflow of estuarine and river water in the upper layers. Maximum surface and bottom layer velocity magnitude are in the order of 0.25 ms^{-1} and 0.15 ms^{-1}, respectively, one order of magnitude smalller than the transient velocity, in line with previous modelling of the residual circulation in the Galician rias (Carballo, Iglesias, and Castro 2009, 130; Iglesias and Carballo 2009, 94-108).

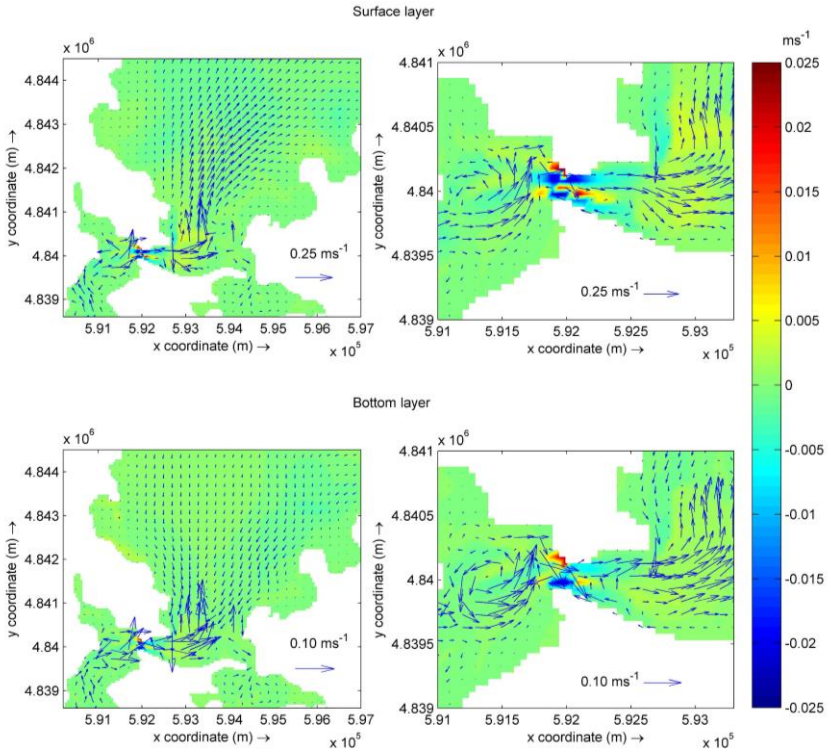

Figure 9. Differences between altered and unaltered residual circulation in Ria de Ortigueira

As is apparent in Figure 9, the modifications of the residual circulation due to energy extraction are concentrated, as in the case of the transient circulation, in the area surrounding the tidal plant. The maximum variations of the velocity magnitude (0.03 ms^{-1}) are of similar importance as in the case of the transient velocity (15% of the unaltered flow), but now the effects can be felt in a wider region (2 km aprox.). Furthermore, the general residual circulation structure is not modified; in particular, the eddy and the positive circulation in the inner and roughly middle and outer ria, respectively, are maintained.

4. Conclusions

This work using as a case study a small estuary located in NW Spain, Ria de Ortigueira, enabled to prove that the operation of a tidal stream farm has an impact both on the transient residual flows. The latter plays a key role at the time to define the hydrodynamic structure of the estuary and drives a important number of environmental processes such as sediment transport, mixing, and pollutant and nutrient transport.

With regard to the transient velocities, the effects can be felt in the vicinity of the tidal farm, with maximum flow alterations of up to 0.3 ms^{-1} (more than 15% of the unaltered flow magnitude). As for the distribution of these effects in the vertical column, the alterations to the transient velocities in the bottom layer are less significant in absolute terms (up to 0.10 ms^{-1}) than those in the surface layer. The effects on the residual circulation are felt in a wider region, as far as 2 km away, approximately double than that of the instantaneous flow, but the variations up to 0.03 ms^{-1}, present the same magnitude, 15% of the unaltered flow. As stated, water level and flow velocity modifications present a different spatial distribution. Whereas water level effects consist of an overall upstream increase with lower downstream variations (predominantly negative), in the case of the flow velocity, its variations significantly differ along the cross sections, in particular in the vicinity of the farm.

In the case of the transient velocity important asymmetry effects are also observed. The inner part of the estuary is flood dominated and therefore, overall, the extraction of the tidal energy is greater during the

flood than during the ebb. Nevertheless, the most important local effects both in tidal levels and current velocities are observed during the ebb, something which is probably due to the complex geometry of the inner and middle ria. With respect to the residual circulation, under unaltered conditions, the Ria de Ortigueira presents a 2D structure in the inner ria, while in the middle and outer ria there exists a more complex 3D circulation pattern with a positive estuarine circulation. Although the alteration of the flow extends to this part of the ria, it is the flow magnitude that is affected; for the general flow patterns are not altered. In particular, the two layer estuarine circulation is maintained. Finally, it is important to note that there have not been observed significant variations between the winter and summer induced circulation, which is probably due to the reduced river discharges into the ria. It should be noted that this is not the case of other Galician rias, where river inflows have been shown to play a major role in the seasonal residual circulation.

In summary, the results obtained show that the operation of the tidal farm modifies the magnitudes of the transient and residual flows, but their general structure is preserved. These impacts may, in turn, lead to other environmental impacts that are outside the scope of this article, such as modifications to the sediment transport patterns; these will be dealt with as a continuation of this line of research.

Acknowledgments

This work constitutes part of the project “Assessment of Renewable Energy Resources” (DPI2009-14546-C02-02) supported by Spain’s Ministry of Science and Innovation (Ministerio de Ciencia e Innovación). Its authors are indebted to M. Alvarez, P. García and M. Ouro for their contribution to the field campaign.

References

Ahmadian, R., R. Falconer, and B. Lin. 2010. Hydro-environmental modelling of proposed severn barrage, UK. *Proceedings of the Institution of Civil Engineers – Energy* 163 (EN3): 107-17.

Ahmadian, Reza, and Roger A. Falconer. 2012. Assessment of array shape of tidal stream turbines on hydro-environmental impacts and power output. *Renewable Energy* 44 (0) (8): 318-27.

Ahmadian, Reza, Roger Falconer, and Bettina Bockelmann-Evans. 2012. Far-field modelling of the hydro-environmental impact of tidal stream turbines. *Renewable Energy* 38 (1) (2): 107-16.

Bahaj, AbuBakr S. 2011. Generating electricity from the oceans. *Renewable and Sustainable Energy Reviews* 15 (7) (9): 3399-416.

Blunden, L. S., and A. S. Bahaj. 2006. Initial evaluation of tidal stream energy resources at portland bill, UK. *Renewable Energy* 31 (2) (2): 121-32.

Carballo, R., G. Iglesias, and A. Castro. 2009. Numerical model evaluation of tidal stream energy resources in the ría de muros (NW spain). *Renewable Energy* 34 (6) (6): 1517-24.

Carballo, R., G. Iglesias, and A. Castro.. 2009. Residual circulation in the Ría de muros (NW spain): A 3D numerical model study. *Journal of Marine Systems* 75 (1-2): 130.

Egbert, G. D., A. F. Bennett, and M. G. G. Foreman. 1994. Topex/Poseidon tides estimated using a global inverse model. *Journal of Geophysical Research* 99 : 24821-52.

Proposal for a Directive Amending Directive 98/70/EC Relating to the Quality of Petrol and Diesel Fuels and Amending Council Directive 93/12/EC and Amending Directive 2009/28/EC on the Promotion of the use of Energy from Renewable Sources [COM(2012) 595](, 2012): .

Iglesias, G., and R. Carballo. 2009. Seasonality of the circulation in the ría de muros (NW spain). *Journal of Marine Systems* 78 (1): 94-108.

Iglesias, G., M. Sánchez, R. Carballo, and H. Fernández. 2012. The TSE index – A new tool for selecting tidal stream sites in depth-limited regions. *Renewable Energy* 48 (0) (12): 350-7.

Myers, L. E., and A. S. Bahaj. 2010. Experimental analysis of the flow field around horizontal axis tidal turbines by use of scale mesh disk rotor simulators. *Ocean Engineering* 37 (2-3) (2): 218-27.

Neill, Simon P., James R. Jordan, and Scott J. Couch. 2012. Impact of tidal energy converter (TEC) arrays on the dynamics of headland sand banks. *Renewable Energy* 37 (1) (1): 387-97.

Ramos, V., R. Carballo, M. Álvarez, M. Sánchez, and G. Iglesias. 2014. A port towards energy self-sufficiency using tidal stream power. *Energy* 71 (0) (7/15): 432-44.

Sanchez, M., R. Carballo, V. Ramos, and G. Iglesias. 2014. Floating vs. bottom-fixed turbines for tidal stream energy: A comparative impact assessment. *Energy* 72 (0) (8/1): 691-701.